# Robust GNSS Multipath Error Modeling based on Deep Quantile Regression with Gaussian Overbounding

Florian Roessl and Omar García Crespillo
*German Aerospace Center (DLR)*

## BIOGRAPHY

**Florian Rößl** received his Master's in Geodesy and Geoinformation from the Technical University Munich in 2022. Since then he is working as a scientific employee at Navigation Department of the German Aerospace Center (DLR). His current field of research includes robust error modeling for safety critical navigation.

**Omar García Crespillo** is currently Group Leader at the Navigation department of the German Aerospace Center (DLR) where he leads activities in GNSS, inertial sensors, integrated navigation systems and integrity monitoring for safe ground and air transportation systems. He received the Ph.D. degree in Robotics, Control and Intelligent Systems from the Swiss Federal Institute of Technology Lausanne (EFPL), Switzerland, and the M.Sc. (Ing.) in Telecommunication Engineering from the University of Málaga, Spain. He was the recipient of the SESAR Young Scientist Award in 2022 and the Early Career Award of the IEEE Aerospace and Electronics Systems Society in 2023.

## ABSTRACT

Safety-critical navigation applications require safe localization error characterization. This requirements extends toglobal navigation satellite systems (GNSS), which are essential for on-board based navigation solutions for different transportation applications. Existing integrity monitoring systems, such as satellite-based augmentation systems (SBAS) or advanced receiver autonomous integrity monitoring (ARAIM), are only capable of providing a robust signal-in-space error description for civil aviation. However, for land-based applications, the local GNSS error, in particular multipath error, due to harsh environments, remains a critical challenge. In this work, an artificial intelligence (AI)-based GNSS code multipath error overbound model for safe error distribution characterization is presented. Two main contributions are made: First, a quantile regression loss function is designed to predict conservative quantiles based on a neural network, so that they are compatible for safety purposes. Second, the quantiles are used to obtain a Gaussian overbound, which describes the underlying error with a parametric distribution that ensures error bounding conditions. The proposed algorithm is first validated with a simple simulation example. Its use and benefit for multipath error modeling is then evaluated with real GNSS data in railway application. Results suggest the capability of this algorithm to reliably characterize multipath errors in challenging scenarios. The method and algorithm can be used for robust multipath distribution characterization in combination with positioning and integrity monitoring algorithms, such as horizontal-ARAIM for railway signaling.

## I. INTRODUCTION

In the context of safety-critical transportation applications, it is essential to ensure that localization errors are properly characterized and bounded. In particular, GNSS are expected to serve as a fundamental component in the development of onboard-based sensor localization solutions for both existing and emerging applications. One example is the use of satellite technology in railway signaling and train control to reduce costs and to enhance the efficiency of railway transportation. For safety or liability related operations, the satellite-based positioning is also required to meet certain integrity requirements, where an important aspect is the safe localization error quantification and threat monitoring.

In civil aviation, augmentation systems are used to ensure navigation integrity. Examples are ground-based augmentation system (GBAS), SBAS or aircraft-based augmentation system (ABAS). Those systems ensure safety by the provision of rigorous error and threat models of satellite orbit and clock, troposphere or airborne multipath.

However, for applications in GNSS harsh environments, such as in urban or land scenarios, the local GNSS error behavior is highly complex. In particular, multipath error is dependent on the local environment, antenna setup, receiver configuration and user dynamics, which is constantly changing. Current GNSS approaches for error modeling based on Gaussian cumulative distribution function (CDF) overbounding cannot be directly applied, since there is not a *one model* that serves all situations and the sample error distribution is not directly observable during operation. The rigorous characterization of multipath in these scenarios remains a critical challenge.

The literature proposes various strategies to address GNSS multipath for different applications. Different techniques have been investigated to mitigate or correct the impact of multipath, including specific antennas design (Teunissen & Montenbruck, 2017) and materials (Caizzone et al., 2023), advanced receiver correlators (Siebert et al., 2023), fault detection and exclusion (FDE) mechanisms (Crespillo et al., 2022) or robust estimators (Crespillo et al., 2020). Other techniques that derived error models for challenging GNSS scenarios are still to be proven rigorous and satisfying bounding conditions (Damy et al., 2016; Groves, 2011; Medina et al., 2018).

In recent years, AI have also demonstrated remarkable results in the GNSS domain. For instance, mitigation of multipath error via Support-Vector Machines (Lee et al., 2023) or the detection of Non-line of sight using logistic regression (García Crespillo et al., 2023). In (No & Milner, 2021) and (Liu & Jiang, 2024) the authors proposed to use a single quantile estimation to quantify the multipath error. However, none of these approaches appear flexible enough, since it makes strong assumption of underlying Gaussian conditions, to account for the high complexity while also providing rigorous error descriptions.

In this work, we propose a methodology based on learning algorithms able to provide a conservative multipath error distribution estimation via deep quantile regression (DQR) combined with CDF overbounding using multiple features derived from commercial off-the-shelf (COTS) GNSS post-correlation observations. The approach is validated by both a simplified simulation data example and by real GNSS data collected on a train.

This paper is organized as follows: Section II introduces a general method for the characterization of a target value distribution based on conservative DQR combined with Gaussian overbounding. The application of the proposed method for the GNSS code multipath error is presented in Section III and an exemplary validation with real GNSS railway data is shown in Section IV, where the proposed model is used in an adapted Horizontal ARAIM algorithm for integrity monitoring. Conclusion are given in Section V along with some possible future research topics.

## II. LEARNING-BASED ROBUST ERROR MODELING

The following section presents an AI-based methodology for safe distribution modeling. The overall objective of the work is to obtain a simple and safe characterization of an unknown distribution $p_{\mathcal{Y}}$ of the target variable $\mathcal{Y}$ in the case the distribution itself is not directly observable. We propose utilizing AI to derive a safe description $p_{\mathcal{Y}|\mathcal{X}}$ based on selected features $\mathcal{X}$ that have been demonstrated to be valuable for describing $\mathcal{Y}$. The methodology involves two steps. First, a conditional distribution is estimated via a neural network. Subsequently, Gaussian overbounding is applied to the model output, in order to obtain a simple to use and safe parametric description.

An AI based algorithm relying on supervised-learning is applied to obtain a fine and robust description of the target $\mathcal{Y}$ via quantile regression. A possible solution is DQR, providing fine and flexible characterization of the true but unknown probability distribution function (PDF) $p_{\mathcal{Y}}(y)$ through its CDF $F_{\mathcal{Y}}$ by means of a set of discrete quantile levels $\mathcal{T} \subseteq (0, 1)$ estimated via a neural network (NN). The quantile $q_\tau$ with probability-level $\tau$ of random variable $\mathcal{Y}$ or the inverse of the CDF (iff strictly monotonically increasing) is defined as:

$$F_{\mathcal{Y}}^{-1}(\tau) = \inf \{y \in \mathbb{R} : \tau \leq F_{\mathcal{Y}}(y)\} = q_\tau, \tag{1}$$

with:

$$F_{\mathcal{Y}}(y) = \int_{-\infty}^{y} p_{\mathcal{Y}}(t)dt. \tag{2}$$

This methodology has been shown to be flexible as it does not rely on assumptions of the underlying distribution (Fakoor et al., 2021). For safety related reasons an overbounding description $\overline{F}$ of the error is required. A CDF overbounding can be expressed as (Rife & Gebre-Egziabher, 2007):

$$\begin{aligned} F_{\mathcal{Y}}(y) \leq \overline{F}(y), \qquad \forall y \mid F_{\mathcal{Y}}(y) \leq \frac{1}{2} \\ F_{\mathcal{Y}}(y) \geq \overline{F}(y), \qquad \forall y \mid F_{\mathcal{Y}}(y) > \frac{1}{2}. \end{aligned} \tag{3}$$

These conditions can be, using the curly-inequality notation of (Rife & Gebre-Egziabher, 2007), also expressed as:

$$p_{\mathcal{Y}}(y) \prec \overline{p}(y). \tag{4}$$

Hence, we can formulate the goal of the work as:

$$p_{\mathcal{Y}}(y) \prec \hat{p}_{\mathcal{Y}|\mathcal{X}}(y) \prec p_{\text{ob}}(y), \qquad \forall y \mid \varepsilon \leq F_{\mathcal{Y}}(y) \leq 1 - \varepsilon, \tag{5}$$

where $\hat{p}_{\mathcal{Y}|\mathcal{X}}$ is an empirical distribution obtained via estimated quantiles $\hat{q}_\tau$ of $\tau$ probability level, $p_{\text{ob}}(y) = \frac{1}{\sqrt{2\pi}\sigma} \exp\left(-\frac{(y-b)^2}{2\sigma^2}\right)$ is a Gaussian overbounding distribution parameterized by bias $b$ and standard deviation $\sigma$ and $\varepsilon = \tau_1$ is the probability margin not covered by the quantiles, which can be associated to the smallest quantile. Although not necessary, we will assume here for simplicity that the selection of quantiles is performed in pair and symmetrically around 0.5 probability to comply with (5). A neural network is applied for approximating the mapping function $g^*_\tau(\mathbf{x};\boldsymbol{\theta}) = F^{-1}_{Y|X=x}(\tau)$ between input features $\mathbf{x} \in \mathcal{X} \subseteq \mathbb{R}^H$ of dimension $H \in \mathbb{Z}$ and quantiles of the target value $y \in \mathcal{Y} \subseteq \mathbb{R}^1$ by learning from training data. The model learns the relationship $\mathcal{Y} \mid \mathcal{X} = \boldsymbol{x}$ between input and target value from experience, which is given in form of noisy observations of the process to be modeled. Because of that, a sufficiently large amount of input-output pairs $\mathcal{D} = \{(\mathbf{x}_n, y_n)\}_{n=1}^N$ with sample size $N$, also denoted as dataset, must be used to ensure representativeness. A deep neural network or multilayer perceptron (MLP) of depth $L$ can be written as (Murphy, 2022):

$$y = g(\mathbf{x};\boldsymbol{\theta}) = g_L(g_{L-1}(\ldots(g_1(\mathbf{x}))\ldots)), \tag{6}$$

where $g_l(\mathbf{x},\boldsymbol{\theta})$ is $l^{\text{th}}$-layer function. The model parameters $\boldsymbol{\theta} = \{\boldsymbol{\omega}, \mathbf{b}\}$, with model weights $\boldsymbol{\omega}$ and bias $\mathbf{b}$, are optimized during the training or learning process with respect to an objective function $\mathcal{J}(\boldsymbol{\theta})$ using a loss function $\mathcal{L}(\mathbf{x}, y)$ to relate model output $\hat{y}$ and target value $y$.

### 1. Conservative Deep Quantile Regression

The authors in (Koenker & Bassett, 1978) proposed the tilted 1-norm, quantile or pinball loss $\mathcal{L}^{QL}_\tau$ for the estimation of quantiles. It can be written as:

$$\begin{aligned}\mathcal{L}^{\text{QL}}_\tau(\zeta) &= \zeta \cdot (\tau - 1) \cdot \mathbb{1}\{\zeta \le 0\} + \zeta \cdot \tau \cdot \mathbb{1}\{\zeta > 0\} \\ &= \max(\underbrace{\zeta \cdot (\tau - 1)}_{\substack{\zeta \le 0 \\ \equiv \\ y < \hat{y}}}, \quad \underbrace{\zeta \cdot \tau}_{\substack{\zeta > 0 \\ \equiv \\ y > \hat{y}}}),\end{aligned} \tag{7}$$

where $\zeta = y - g_\tau(\mathbf{x},\boldsymbol{\theta})$ is the prediction error and $\mathbb{1}\{\zeta < 0\}$ is the indicator function returning 1 iff (if and only if) the condition is fulfilled, or 0 otherwise. In order to derive a safe multipath error characterization is not enough to estimate approximate quantiles, which may result in upper or under estimating the true quantile. For that reason, we propose a penalty to the standard quantile regression loss function with an underestimation loss, such that conservative error estimations become more favorable than underestimation. The underbounding condition based on the quantile level $\tau$ can be noted as equations:

$$u(\hat{y}, y; \tau) = \begin{cases} \mathbb{1}\{y < \hat{y}\}, & \text{if } \tau < 0.5, \\ \mathbb{1}\{0\}, & \text{if } \tau = 0.5, \\ \mathbb{1}\{y > \hat{y}\}, & \text{otherwise.} \end{cases} \tag{8}$$

Combing Equation 7 and Equation 8 the underestimated quantile loss $\acute{\mathcal{L}}_{\text{UQ},\tau}$ can be written as:

$$\acute{\mathcal{L}}_{\text{UP},\tau}(\zeta) = \begin{cases} |\min(\zeta, 0)|, & \text{if } \tau < 0.5, \\ 0, & \text{if } \tau = 0.5, \\ |\max(\zeta, 0)|, & \text{otherwise.} \end{cases} \tag{9}$$

However, the magnitude of the extracted loss $\acute{\mathcal{L}}_{\text{UP},\tau}$ is dependent on $\tau$, since the error $\zeta$ is scaled by $\tau$. For this reason, we propose to normalize the error by the inverse of the quantile in order to penalize each quantile-level equally, including the median. The normalization factors for the left $c_{\text{ob,l}}$ and right $c_{\text{ob,r}}$ side of the distribution are written as:

$$c_{\text{ob,l}}(\tau) = \begin{cases} \dfrac{1}{|\tau - 1|}, & \text{if } \tau < 0.5, \\ \dfrac{1}{2} \cdot \dfrac{1}{|\tau - 1|}, & \text{if } \tau = 0.5, \\ 0, & \text{otherwise,} \end{cases} \tag{10}$$

and

$$c_{\text{ob,r}}(\tau) = \begin{cases} 0, & \text{if } \tau < 0.5, \\ \frac{1}{2} \cdot \frac{1}{|\tau|}, & \text{if } \tau = 0.5, \\ \frac{1}{|\tau|}, & \text{otherwise.} \end{cases} \tag{11}$$

The conservative quantile loss $\mathcal{L}_\tau^{\text{CQL}}$ can be expressed as:

$$\begin{aligned} \mathcal{L}_\tau^{\text{CQL}}(\zeta) &= \zeta \cdot c_{\text{ob,l}}(\tau) \cdot \tau \cdot \mathbb{1}\{\zeta > 0\} + \zeta \cdot c_{\text{ob,r}}(\tau) \cdot (\tau - 1) \cdot \mathbb{1}\{\zeta \leq 0\} \\ &= \max(\zeta \cdot c_{\text{ob,l}}(\tau) \cdot \tau, \zeta \cdot c_{\text{ob,r}}(\tau)(\tau - 1)) \end{aligned} \tag{12}$$

It can be directly incorporated into the standard quantile loss via:

$$\begin{aligned} \mathcal{L}_\tau(\zeta) &= \mathcal{L}_\tau^{\text{QL}}(\zeta) + \alpha \mathcal{L}_\tau^{\text{CQL}}(\zeta) \\ &= \max(\zeta \cdot (1 + \alpha \cdot c_{\text{ob,l}}(\tau)) \cdot (\tau - 1), \zeta \cdot (1 + \alpha \cdot c_{\text{ob,r}}(\tau)) \cdot \tau), \end{aligned} \tag{13}$$

with the tunable hyperparameter $\alpha$ to scale the penalty of non conservative predictions. Figure 1 visualizes the standard quantile loss, conservative penalty and the combination of both.

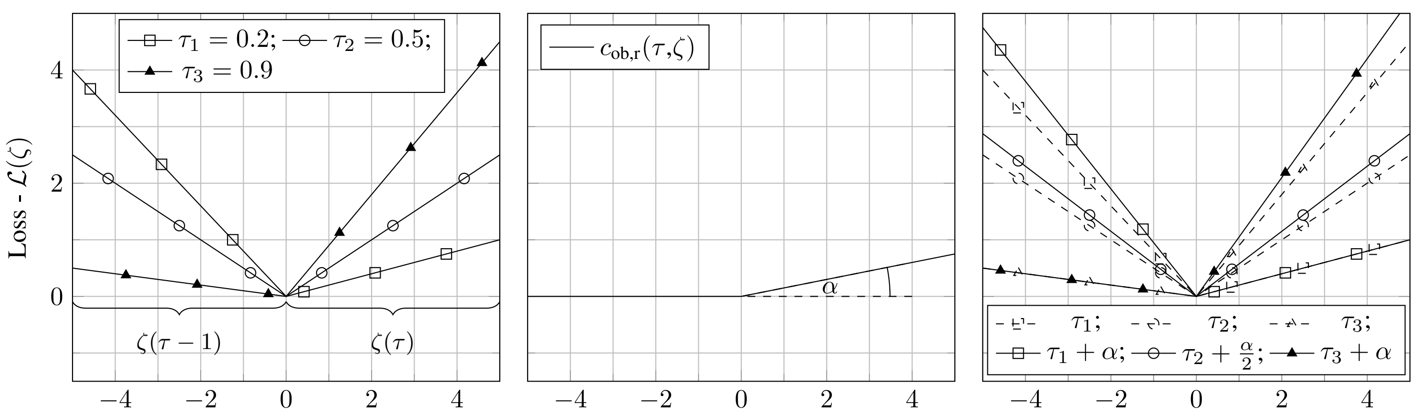


**(a)** Standard quantile loss

**(b)** Underbound loss

**(c)** Combined quantile loss

**Figure 1:** Quantile loss, proposed underbound loss and the combination of both as a function of the prediction error $\zeta$ for three different quantile levels $\{\tau_1 = 0.2, \tau_2 = 0.5, \tau_3 = 0.9\}$.

The final cost or objective function $\mathcal{J}(\boldsymbol{\theta})$ for DQR to be optimized during the learning can be written as:

$$\mathcal{J}(\boldsymbol{\theta}; \mathcal{D}_{\text{train}}) = \frac{1}{|\mathcal{D}_{\text{train}}|} \sum_{(\mathbf{x},y)}^{\mathcal{D}_{\text{train}}} \sum_{\tau}^{\mathcal{T}} \mathcal{L}_\tau(y - g_\tau(\mathbf{x}; \boldsymbol{\theta})) + \beta \cdot \mathcal{P}(\mathcal{T}, \mathcal{D}_{\text{train}}) + \gamma \cdot \boldsymbol{\omega}^T \boldsymbol{\omega}, \tag{14}$$

with the non crossing constraint penalty $\mathcal{P} = \sum_{(x,y)}^{\mathcal{D}_{train}} \sum_{\tau}^{|\mathcal{T}|-1} \max\left(f_{\tau_t}(\mathbf{x}) - f_{\tau_{t+1}}(\mathbf{x}) + \nu, 0\right)$ for preventing quantile intersections with the minimum distance $\nu$ and tunable hyperparameter $\gamma$ for the weight-decay (Fakoor et al., 2021).

## 2. Quantile based Gaussian Overbounding

Next, the predicted quantiles are overbounded with a Gaussian distribution in order to obtain a parametric error characterization. This is done in two steps following the method in Blanch et al. (2019), using not empirical data but predicted quantiles instead. The quantiles can also be interpreted as a direct representation of the histogram without the need to bin the empirical data into a histogram, which avoids the introduction of discretization errors.

First, an intermediate symmetric unimodal overbounding distribution $F_{\text{su}}$ is determined based on $\mathcal{T}_{\text{su}}$. In detail, quantiles $\bar{q}_{\tau,\text{su}}$ are determined in order to satisfy symmetry and unimodal constraints, with $\bar{q}_{\tau,\text{su}} \geq \hat{q}_\tau$. Next a Gaussian overbounding distribution $F_{\text{ob}}$ is created, with parameters $\mu = \overline{q}_{\tau=0.5,\text{su}}$ and the bounding standard deviation is found with the half interval search (Blanch et al., 2019). Hence, it can be written as:

$$F(y) \leq F_{\text{su}}(y) \leq \overline{F}_{\text{ob}}(y), \qquad \forall y \leq 0. \tag{15}$$

This step is conducted separately for the *left*, using $\mathcal{T}_{\text{su,left}} = \{\tau \in \mathcal{T} : \tau \leq 0.5\}$ with $+\hat{q}_\tau$, and *right*, using $\mathcal{T}_{\text{su,right}} = \{\tau \in \mathcal{T} : \tau \geq 0.5\}$ with $-\hat{q}_\tau$, side of the predicted distribution. The parameters of the final bound $F_{\text{ob}}(y; b, \sigma)$ are determined via the maximum operation:

$$\begin{aligned} b &= \max(|\mu_{\text{left}}|, |\mu_{\text{right}}|), \\ \sigma &= \max(\sigma_{\text{left}}, \sigma_{\text{right}}). \end{aligned} \tag{16}$$

Now we can write:

$$p_{\mathcal{Y}}(y) \prec p_{\text{ob}}(y; b, \sigma). \tag{17}$$

Figure 2 illustrates the bounding process of the true but unknown distribution $F_y$ via predicted quantiles $\hat{q}_\tau$ and the Gaussian overbound $F_{\text{ob}}$.

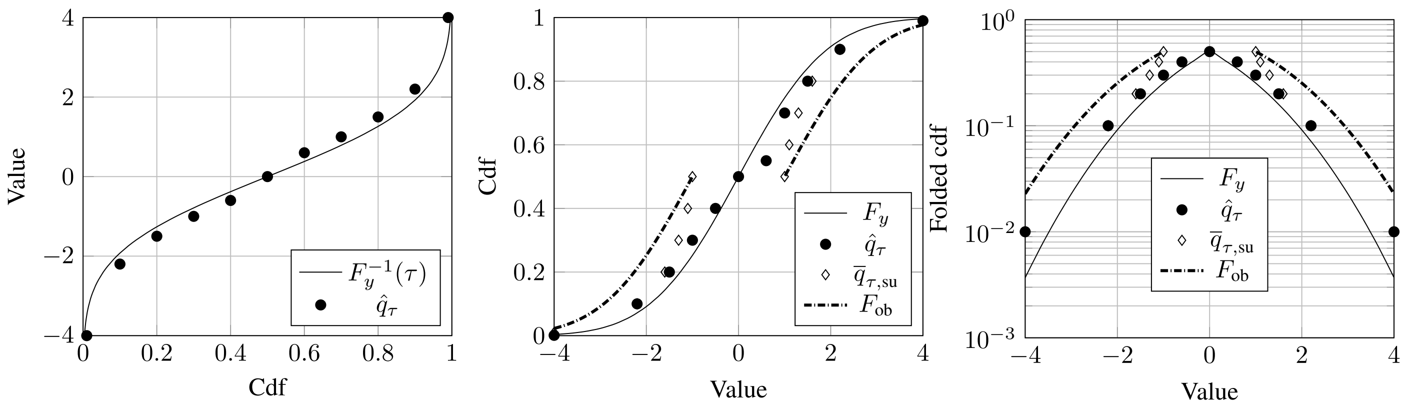


**(a)** Predicted conservative quantiles

**(b)** Symmetric unimodal quantiles and Gaussian overbound

**(c)** Gaussian overbound plotted as folded cdf

**Figure 2:** CDF overbounding of true distribution $F_y$ with $F_{\text{ob}}$ based on predicted quantiles $\hat{q}_\tau$ and intermediate symmetric and unimodal quantiles $\overline{q}_{\tau,\text{su}}$.

## 3. Simulation based Verification

In a first experiment, simulation data with a known distribution, generated using a Gaussian mixture model, is employed to evaluate the capability of the methodology in estimating conservative quantiles. For the experiment the dataset is generated by sampling from $y(x) \sim \sum_{i=1}^{2} \pi_i \mathcal{N}(0, \sigma_i(x)$ with weight vector $\boldsymbol{\pi} = [0.8, 0.2]^T$ and standard deviation vector $\boldsymbol{\sigma} = [-2x + 5, -4x + 10]^T$ where $x \sim \mathcal{U}(1, 2)$. A sample dataset $\mathcal{D}_{\text{train}}$ of size $1 \times 10^5$ is used for training a neural network for 100 epochs. In the experiment, two models are trained: one applying the proposed underbound penalty from (12) with $\alpha = 0.15$ and one without it.

Figure 3 shows the generated dataset in Figure 3a and experimental results in Figure 3b of the simulation based experiment. In the zoomed window one can observe that predicted quantiles without an underbound loss $\hat{q}_\tau(y|x)$, marked by the triangle, are not able to safely describe neither the empirical $F_{\text{data}}^{-1}$ nor the true inverse cdf $F^{-1}$, however predicted quantiles using an underbound loss, marked by filled circle, are able to provide a safe estimation. For evaluation the conservative error $\hat{\epsilon}_{\text{con}}$ is used, which considers the sign of the prediction with respect to the quantile level with respect to the definition of conservatism. It is given by:

$$\hat{\epsilon}_{\text{con}} = \begin{cases} \hat{q}_\tau - q_\tau, & \text{if } \tau < 0.5, \\ 0, & \text{if } \tau = 0.5, \\ q_\tau - \hat{q}_\tau, & \text{else.} \end{cases} \tag{18}$$

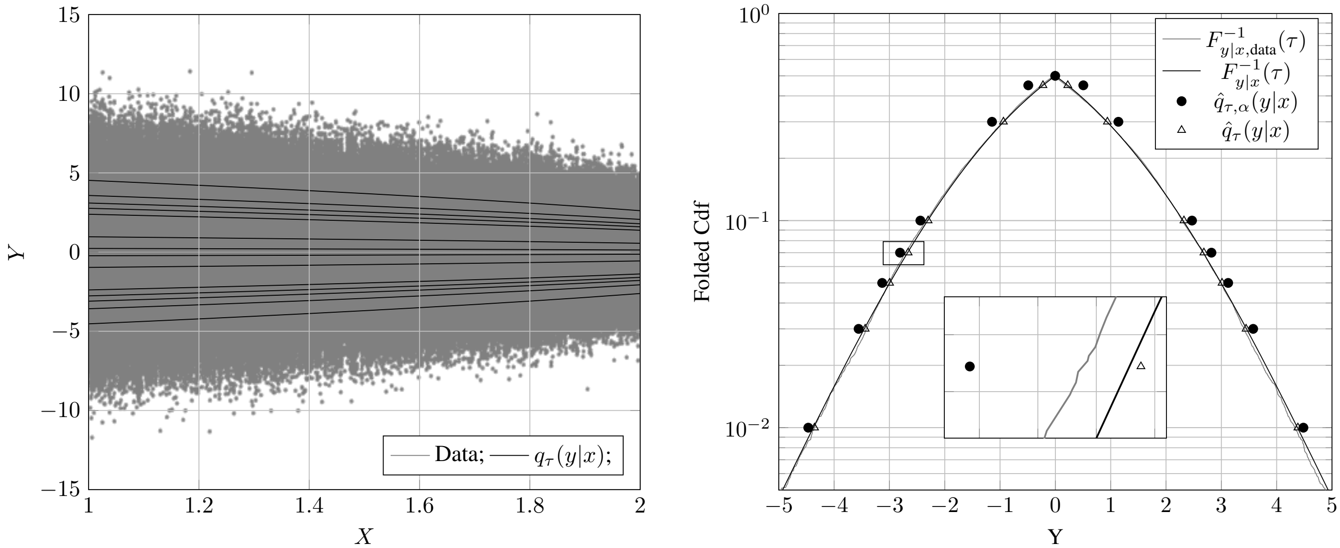


**(a)** Toy dataset with true conditional quantiles $q_\tau(y|x)$

**(b)** Prediction results of $f(y|x = 1.1)$ after successful training

**Figure 3:** Multi-Gaussian simulation dataset with true and empirical distribution and predicted quantiles. Two experiments are made once using the proposed underbound loss estimating $\hat{q}_{\tau,\alpha}$ and once not using it estimating $\hat{q}_\tau$.

In both experiments the model predicts the quantile set $\mathcal{T} = \{0.01, 0.03, \cdots, 0.07, 0.1, 0.2, \cdots 0.4, 0.45, 0.5, 0.55, 0.6, 0.7 \cdots 0.9, 0.93, 0.95, \cdots 0.99\}$, with $\alpha$ indicating whether the conservatism loss is used or not. Table 1 provides a statistical summary of the simulation based experiments using the underbound penalty with $\alpha = 0.15$ and without using it. The first and second row summarizes quantile predictions $\mathcal{T}_{\overline{\mathbb{M}}} = \mathcal{T} \setminus \{\tau_{\text{med}}\}$ excluding the median, since no conservatism is defined for that quantile. The results validate the use of the underbound loss to obtain a safe quantification of the conditional probability. In particular, the prediction errors for quantiles $\mathcal{T}_{\overline{\mathbb{M}}}$ without the median, are larger as indicated by the mean. However, these predictions are conservative, as indicated by the minimum error, which remains positive, meaning that all predictions are safe. Furthermore, the use of the underbound loss does not affect the prediction quality for estimating the median, as the statistical values for $\mathcal{T}_{\mathbb{M},\alpha}$ and $\mathcal{T}_{\mathbb{M}}$ remain largely consistent.

**Table 1:** Statistical error summary of the multi-Gaussian simulation based experiment.

| | Mean | Min | Max | Std. |
|---|---|---|---|---|
| $\mathcal{T}_{\overline{\mathbb{M}},\alpha}$ | $0.1423$ | $0.0826$ | $0.2903$ | $0.0456$ |
| $\mathcal{T}_{\overline{\mathbb{M}}}$ | $0.0116$ | $-0.0533$ | $0.1077$ | $0.0198$ |
| $\mathcal{T}_{\mathbb{M},\alpha}$ | $-0.0035$ | $-0.0074$ | $-0.0021$ | $0.0011$ |
| $\mathcal{T}_{\mathbb{M}}$ | $-0.0053$ | $-0.0073$ | $-0.0019$ | $0.0012$ |

## III. ROBUST GNSS MULTIPATH ERROR MODELING

The following section presents the application of the proposed methodology to model GNSS code multipath error. Figure 4 shows a schematic overview of the method for GNSS multipath error modeling. First, a model is trained offline using manually selected features derived from historic GNSS data, which allows the incorporation of expert knowledge. After successful training, the model can be deployed for real-time applications providing a multipath error bound modeled as a parametric *CDF-overbounded* distribution.

In order to apply the deep quantile regression, it is essential to obtain suitable input features $\boldsymbol{x}$, and the corresponding target value, $y$, representing the observed error. In this work, the input features are selected based on GNSS observables, as follows:

- **Carrier-to-noise ratio** $C/N_0$ $[\mathrm{dB\,Hz}]$: is the signal strength observation of the tracked signal,
- **Elevation angle** $\theta$ $[\mathrm{deg}]$: of the tracked satellite on the local horizon,

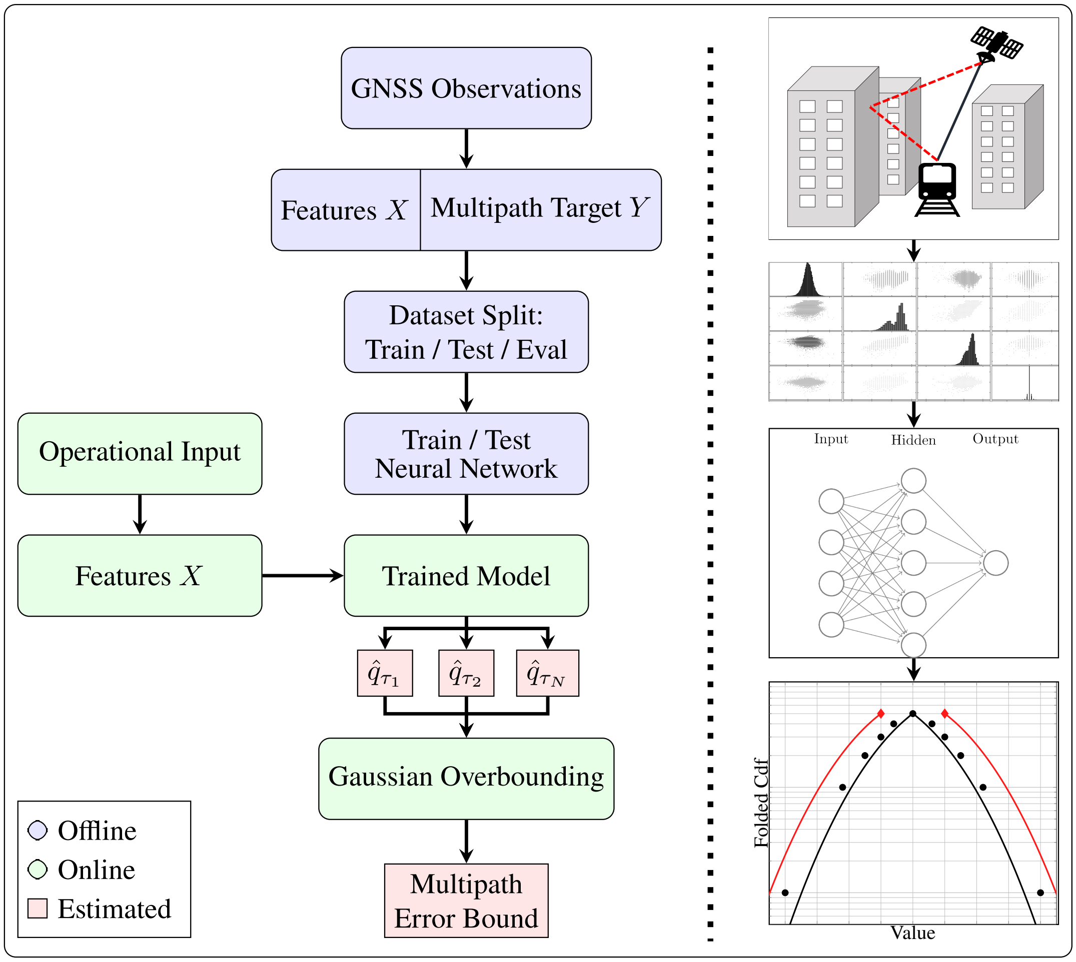


**Figure 4:** Scheme of proposed method for multipath error quantification

- **Pre-normalized** $\overline{C/N_0}$ $[-]$: is normalized with respect to the elevation angle of the observed satellite using a fitted model,
- **Change rate of** $\Delta C/N_0$ $[\mathrm{dB\,Hz\,s^{-1}}]$: over time to capture the temporal evolution of the signal strength,
- **Lock time** $t_{\mathbf{lock}}$ $[\mathrm{s}]$: of a tracked signal,
- **Number of tracked signals** $N_{\mathbf{signals}}$ $[\#]$: of different frequencies for the specific satellite,
- **Pseudorange consistency** $\overline{\mathbf{PRC}}[\mathrm{m\,s^{-1}}]$: is the difference of the pseudorange change rate and the change rate derived from the Doppler observation $f_{\text{Doppler}}$, being defined as $\overline{\text{PRC}} = \frac{\Delta\rho}{\Delta t} - f_{\text{Doppler}} \cdot \lambda$ (Lee et al., 2023),
- **Permanent multipath error bound** $\sigma_{\mathbf{perm}}$ $[\mathrm{m}]$: an elevation dependent error bound model for the description of the multipath error caused by immediate environment of the permanent antenna installation (Kliman et al., 2024).

The target value $y$, describing the GNSS code multipath error, is modeled via the Code-Minus-Carrier linear combination (Braasch, 1994). This approach offers the advantage of obtaining a simple multipath observation, but it also has the disadvantage of combining code and phase multipath with noise. Furthermore, the windowing size used for mean removal is crucial for the quality of the multipath observation (Caamano et al., 2020; Roberto Matera et al., 2024).

## IV. EXPERIMENTAL VALIDATION WITH RAILWAY GNSS MULTIPATH

For experimental validation estimating GNSS multipath error bounds a real scenario railway sensors dataset is used. The dataset was collected in the context of the European research project *Railgap*.

## 1. Measurement Campaign

The data utilized for the training, testing, and evaluation of the methodology includes multi-frequency GPS and Galileo observations collected with a *Javad Delta-3* GNSS receiver equipped with a *Antcom G8Ant-3A4TB1* antenna in the vicinity of Málaga, Spain. Figure 5 shows the train and GNSS antenna installation used for sensor data collection as well as the campaign area. The complete dataset comprises six batches of data collected between February 2023 and February 2024, encompassing approximately $1300\,\mathrm{km}$.


**(a)** Plasser & Theurer draisine **(b)** GNSS antenna installation on a pole **(c)** Campaign area

**Figure 5:** Train used for data collection, actual antenna installation and campaign area map in Málaga during EU project Railgap

For evaluation of the experiments a train run from Cártama to Álora recorded at 2023-05-17 between 09:38 to 09:58 is studied.

## 2. Network Architecture and Training Process

In accordance with Occam's razor, the architectural design of the model is kept as simple as possible. A four-layer MLP with hyperbolic tangent (Tanh) activation is selected, and batch normalization is applied. For regularization purposes, weight decay and dropout with $p = 0.25$ are applied. The model parameters are optimized with the Adam optimizer during training for 200 epochs and the best model is selected based on the minimum test loss. For training we use a *Nvidia RTX A4000* GPU with $12\,\mathrm{GB}$ equipped with *Intel Xeon Core* CPUs and 64GB RAM. For each GNSS constellation and frequency, a distinct model is trained separately.

## 3. Robust Multipath Error Overbounding

After successful training the models performance is studied on the evaluation dataset. Figure 6 gives a qualitative impression of the models prediction performance. Isolated multipath observations are plotted along with predicted quantiles for the evaluation dataset for two exemplary GPS and Galileo satellites. One can observe that the trend of the isolated multipath error is well characterized by predicted quantiles.

In a next step, the overall performance of the method is studied. Kfold cross validation (CV) Murphy, 2022, with $k = 5$, is applied on the training/testing dataset, in order to obtain more reliable results. This consists of selecting $k$ different combinations of the training and testing datasets, in order to obtain more robust results. Furthermore, three different set of quantiles $\mathcal{T}_1$ with $\tau_1 = 1 \times 10^{-3}$, $\mathcal{T}_2$ with $\tau_1 = 1 \times 10^{-4}$ and $\mathcal{T}_3$ with $\tau_1 = 1 \times 10^{-5}$ are studied, to investigate the impact of the probability margin on the prediction quality. Figure 7 shows the folded cdf of multipath observations normalized with respect to the predicted error overbound via $\overline{y} = \mathrm{sgn}(y) \cdot \frac{\max\left(|y| - \hat{b}_{\text{mpn}}, 0\right)}{\hat{\sigma}_{\text{mpn}}}$ for GPS (first column) and Galileo (second column) estimating $\hat{q}_{\tau_1 = 1\times10^{-3}}$ (first row), $\hat{q}_{\tau_1 = 1\times10^{-4}}$ (second row) and $\hat{q}_{\tau_1 = 1\times10^{-5}}$ (third row). For all shown experiments, the method is able to provide a safe description for the training, testing and evaluation dataset within the prediction interval defined by $\tau_1$ and $\tau_M$ with $M$ quantiles, since the standard normal distribution is able to overbound all curves down to the specified prediction interval.

Table 2 gives a quantitative summary of the maximum fault rate of the CV for selected confidence intervals ($k\sigma$), with a fault being defined as $\mathbb{1}\left\{|y| > b + k\sigma\right\}$. It can be observed, that the models are able to provide a safe error description for all confidence intervals up to the specified prediction interval, because the probability mass not covered by the confidence interval is larger than the corresponding fault rate for all instances.

## 4. Preliminary Analysis via modified H-ARAIM

An exemplary application of the error model, with $\tau_1 = 1 \times 10^{-4}$, is given in this section. The robustness of the proposed method to provide a safe error description is investigated with a modified H-ARAIM algorithm similarly to Rößl et al., 2023.

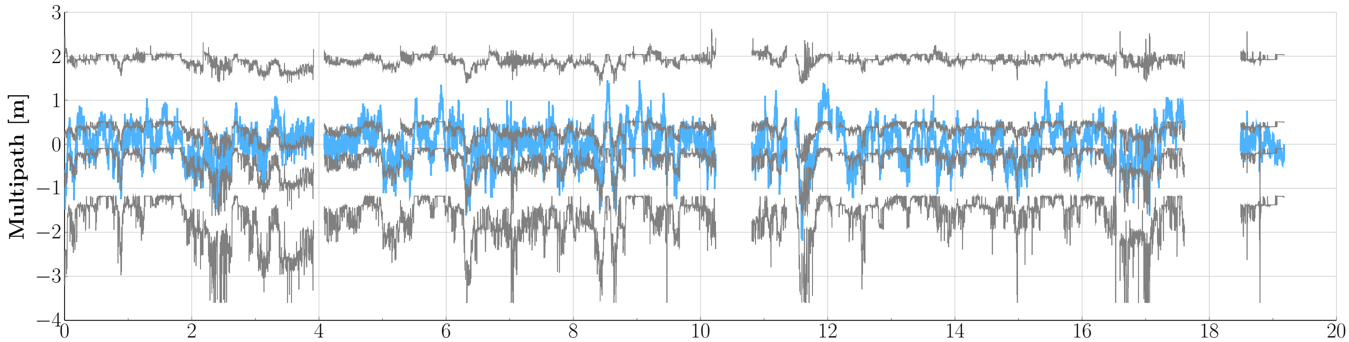


**(a)** GPS SVID-26

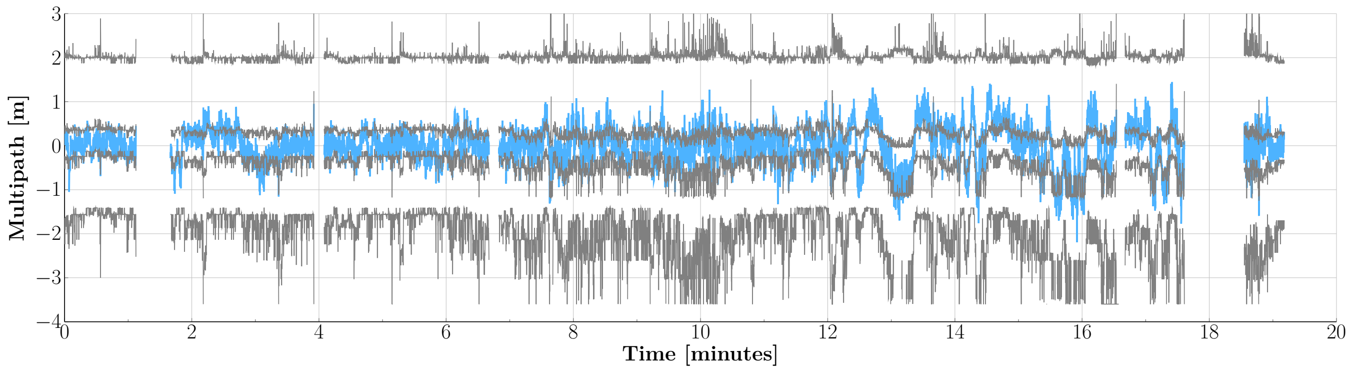


**(b)** Galileo SVID-13

**Figure 6:** Predicted error quantiles $\left\{\hat{q}_{\tau_1=1\times10^{-4}}, \hat{q}_{\tau_2=0.2}, \hat{q}_{\tau_3=0.8}, \hat{q}_{\tau_{\text{end}}=0.9999}\right\}$ (gray), observed multipath (blue) for exemplary GPS and Galileo satellites using the models trained on $\mathcal{T}_2$

**Table 2:** Maximum fault rate of K-Fold models in percent [%] per confidence interval $(k \cdot \sigma)$ for GPS and Galileo evaluation dataset covered by $b_{\text{ob}} + k \cdot \sigma_{\text{ob}}$ using $\alpha = 0.15$

| Confidence Interval [%] | GPS | | | Galileo | | |
|---|---|---|---|---|---|---|
| | $\tau_1 = 1 \times 10^{-3}$ | $\tau_1 = 1 \times 10^{-4}$ | $\tau_1 = 1 \times 10^{-5}$ | $\tau_1 = 1 \times 10^{-3}$ | $\tau_1 = 1 \times 10^{-4}$ | $\tau_1 = 1 \times 10^{-5}$ |
| 68.27 $(1\sigma)$ | 11.6423 | 9.6480 | 2.1330 | 11.2017 | 8.9723 | 5.8804 |
| 95.45 $(2\sigma)$ | 0.7834 | 0.5968 | 0.0152 | 0.9084 | 0.5436 | 0.2469 |
| 99.73 $(3\sigma)$ | 0.0217 | 0.0065 | 0.0 | 0.0566 | 0.0249 | 0.045 |
| 99.80 $(3.09\sigma)$ | 0.0868 | 0.0043 | 0.0 | 0.0385 | 0.0136 | 0.0045 |
| 99.98 $(3.71\sigma)$ | 0.0 | 0.0 | 0.0 | 0.0068 | 0.0023 | 0.0 |
| 99.998 $(4.26\sigma)$ | 0.0 | 0.0 | 0.0 | 0.0 | 0.0 | 0.0 |

Precise products are applied to correct space and satellite based pseudorange errors as good as possible, such that the remaining range can be attributed to the multipath effect. The modifications made to the baseline H-ARAIM algorithm are presented in Appendix A. The horizontal position error (HPE) is calculated with respect to a post processed kinematic tightly-coupled GNSS/INS solution.

Figure 8 summarizes the H-ARAIM results of the evaluation run in the Stanford plot and the corresponding position dilution of precision (PDOP) versus horizontal protection level (HPL) plot. It can be seen that there is no misleading information obtained for any of the epochs. The error model was able to provide a safe multipath error characterization for all scenarios within the evaluation dataset. The large HPL values can be explained by a worse PDOP value, which indicates that the geometrical constellation is the main driver, rather than the error model as shown in Figure 8c for the presented experiment.

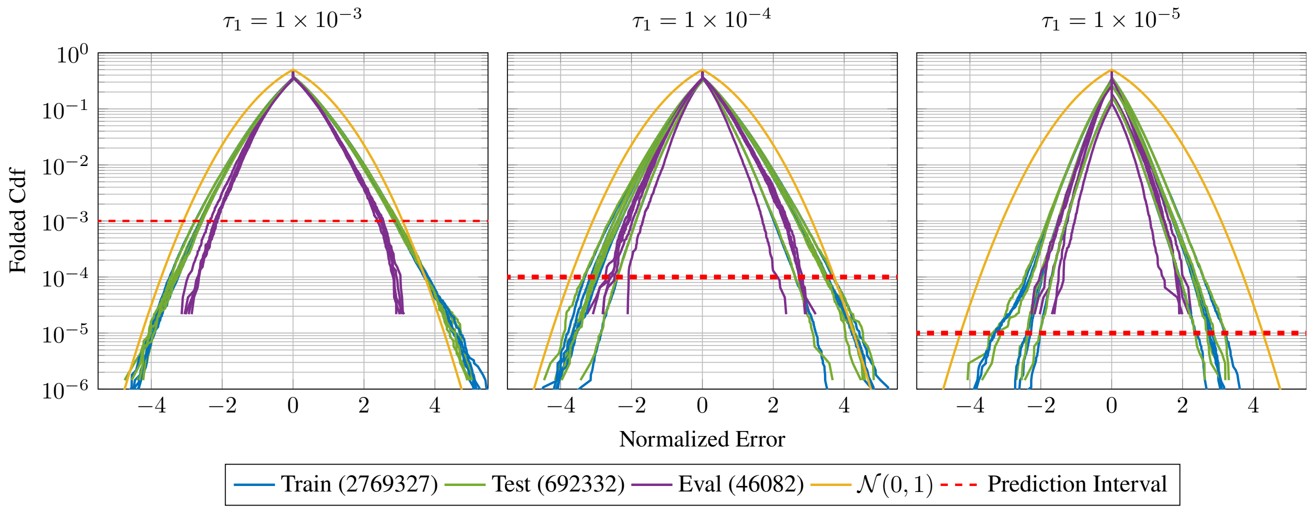


**(a)** GPS

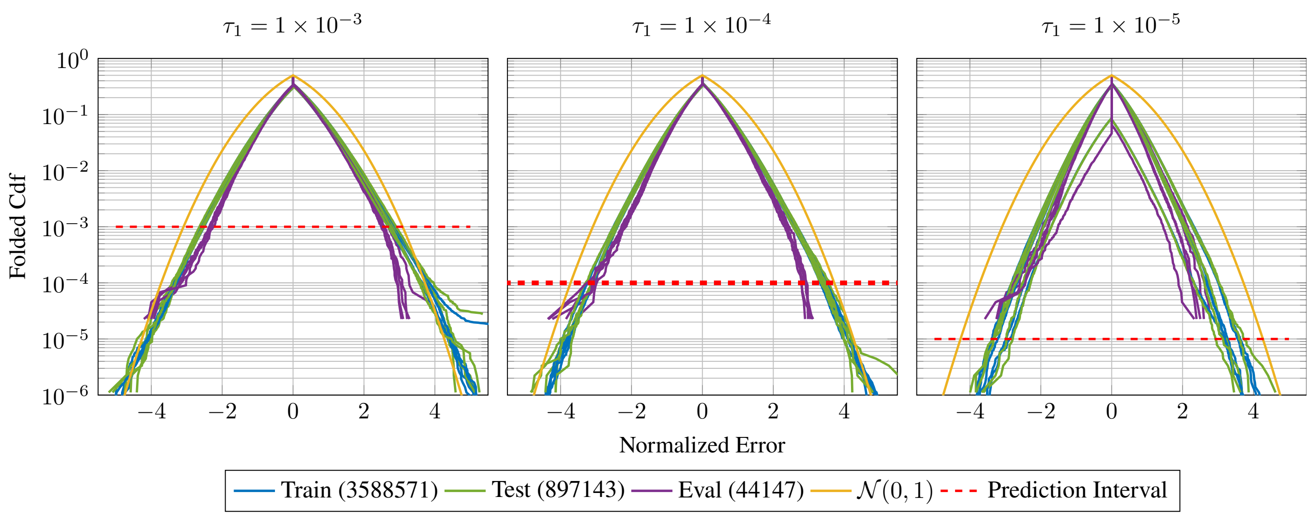


**(b)** Galileo

**Figure 7:** Normalized folded CDF distribution of the K-Fold experiment ($k = 5$) for the GPS and Galileo model. Multipath target values $y$ are normalized by the predicted error bound for train, test and evaluation dataset. The horizontal red dashed line indicates the prediction interval covered by estimated quantiles $\mathcal{T}$.

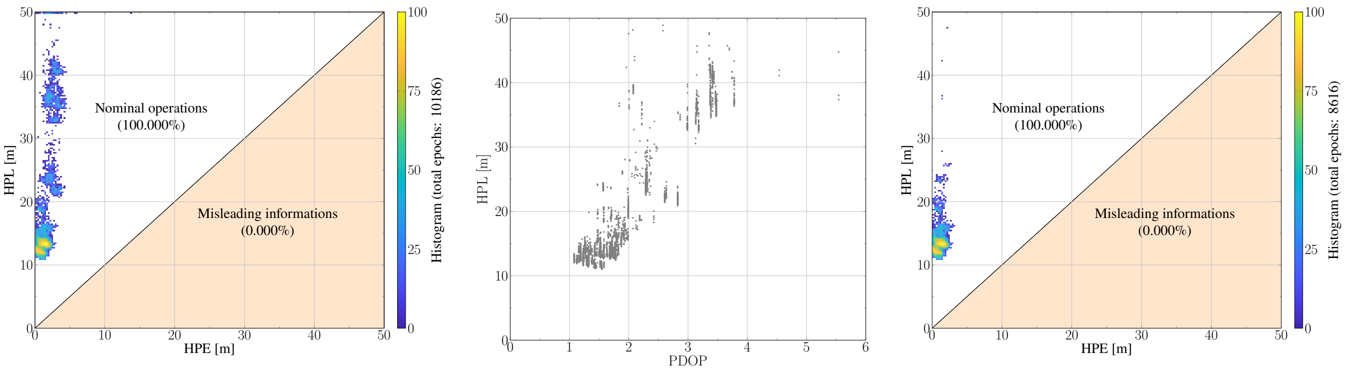


**(a)** Stanford diagram for evaluation dataset **(b)** PDOP versus HPL **(c)** PDOP $\leq$ 2 filtered Stanford diagram

**Figure 8:** Modified H-ARAIM results of the evaluation dataset using the NN-based multipath error model. The Stanford diagram plots estimated HPE versus HPL in a 2-d histogram.

## V. CONCLUSION

In this paper, we present a learning-based GNSS code multipath error modeling approach that provides a robust error characterization via a CDF overbound for close-to-land or land-based navigation applications. In a two-step process, first, conservative quantiles are estimated using deep quantile regression to create an empirical CDF overbound. Second, Gaussian overbounding is used to obtain a simple parametric and safe error model. Simulation-based and real-scenario-based experiments suggests the suitability of the approach to ensure safe error characterization. The proposed methodology can be applied to existing hardware solutions or COTS GNSS receivers, since all features are based on post-correlation GNSS observations. The resulting error model can be used for GNSS integrity monitoring systems, like SBAS, ARAIM or multi-sensor solutions for their adaptation to railway or other land-based applications. The proposed method is not only applicable to the GNSS multipath problem, but it may also be applied to other sensor error modeling problems that require a safe representation of the error, where the relationship between the input and target value cannot be fully modeled. Future work will focus on the refinement of the model architecture and the investigation of the effect quantile resolution.

## ACKNOWLEDGEMENTS

This work has been partly funded by the European Union's Horizon 2020 research and innovation programme under grant agreement No: 101004129 *RAILGAP* project.

## REFERENCES

Blanch, J., Walter, T., & Enge, P. (2019). Gaussian Bounds of Sample Distributions for Integrity Analysis. *IEEE Transactions on Aerospace and Electronic Systems*, *55*(4), 1806–1815. https://doi.org/10.1109/TAES.2018.2876583

Braasch, M. S. (1994). Isolation of GPS Multipath and Receiver Tracking Errors. *Navigation*, *41*(4), 415–435. https://doi.org/10.1002/j.2161-4296.1994.tb01888.x

Caamano, M., Garcia Crespillo, O., Gerbeth, D., & Grosch, A. (2020). Detection of GNSS Multipath with Time-Differenced Code-Minus-Carrier for Land-Based Applications. *2020 European Navigation Conference (ENC)*. https://doi.org/10.23919/enc48637.2020.9317340

Caizzone, S., Gerguis, R. A., Addo, E. O., Hehenberger, S. P., & Elmarissi, W. (2023). Spatial Filtering of Multipath at GNSS Reference Stations through Metamaterial-Based Absorbers. *IEEE Transactions on Aerospace and Electronic Systems*, 1–10. https://doi.org/10.1109/TAES.2023.3294896

Crespillo, O. G., Andreetti, A., & Grosch, A. (2020). Design and Evaluation of Robust M-estimators for GNSS Positioning in Urban Environments. *Proceedings of the 2020 International Technical Meeting of The Institute of Navigation*, 750–762. https://doi.org/10.33012/2020.17211

Crespillo, O. G., Grosch, A., Adjroloh, P. H., Zhu, C., Capua, R., Frittella, F., & Kutik, O. (2022). Multisensor Localization Architecture for High-Accuracy and High-Integrity Land-based Applications. *Proceedings of the 35th International Technical Meeting of the Satellite Division of The Institute of Navigation (ION GNSS+ 2022)*, 1873–1889. https://doi.org/10.33012/2022.18539

Damy, S., Majumdar, A., & Ochieng, W. Y. (2016). GNSS-based High Accuracy Positioning for Railway Applications. *Proceedings of the 2016 International Technical Meeting of The Institute of Navigation*, 1003–1014. https://doi.org/10.33012/2016.13479

Fakoor, R., Kim, T., Mueller, J., Smola, A. J., & Tibshirani, R. J. (2021). Flexible Model Aggregation for Quantile Regression. https://doi.org/10.48550/arXiv.2103.00083

García Crespillo, O., Ruiz-Sicilia, J. C., Kliman, A., & Marais, J. (2023). Robust design of a machine learning-based GNSS NLOS detector with multi-frequency features. *Frontiers in robotics and AI*, *10*, 1171255. https://doi.org/10.3389/frobt.2023.1171255

Groves, P. D. (2011). Shadow Matching: A New GNSS Positioning Technique for Urban Canyons. *Journal of Navigation*, *64*(3), 417–430. https://doi.org/10.1017/S0373463311000087

Kliman, A., Grosch, A., & García Crespillo, O. (2024). Permanent train-side GNSS multipath characterization considering time-correlation for safe railway localization. *2024 European Navigation Conference (ENC)*.

Koenker, R., & Bassett, G. (1978). Regression Quantiles. *Econometrica*, *46*(1), 33. https://doi.org/10.2307/1913643

Landskron, D., & Böhm, J. (2018). VMF3/GPT3: refined discrete and empirical troposphere mapping functions. *Journal of geodesy*, *92*(4), 349–360. https://doi.org/10.1007/s00190-017-1066-2

Lee, Y., Wang, P., & Park, B. (2023). Nonlinear Regression-Based GNSS Multipath Dynamic Map Construction and Its Application in Deep Urban Areas. *IEEE Transactions on Intelligent Transportation Systems*, *24*(5), 5082–5093. https://doi.org/10.1109/TITS.2023.3246493

Liu, R., & Jiang, Y. (2024). Overbounding Multipath Error in Urban Canyon With LSTM Using Multi-Sensor Features. *IEEE Transactions on Intelligent Transportation Systems*, 1–15. https://doi.org/10.1109/TITS.2024.3376812

Medina, D., Gibson, K., Ziebold, R., & Closas, P. (2018). Determination of Pseudorange Error Models and Multipath Characterization under Signal-Degraded Scenarios. *Proceedings of the 31st International Technical Meeting of The Satellite Division of the Institute of Navigation (ION GNSS+ 2018)*, 3446–3456. https://doi.org/10.33012/2018.16094

Montenbruck, O., Steigenberger, P., Prange, L., Deng, Z., Zhao, Q., Perosanz, F., Romero, I., Noll, C., Stürze, A., Weber, G., Schmid, R., MacLeod, K., & Schaer, S. (2017). The Multi-GNSS Experiment (MGEX) of the International GNSS Service (IGS) – Achievements, prospects and challenges. *Advances in Space Research*, *59*(7), 1671–1697. https://doi.org/10.1016/j.asr.2017.01.011

Murphy, K. P. (2022). *Probabilistic Machine Learning: An introduction*. MIT Press. probml.ai

No, H., & Milner, C. (2021). Machine Learning Based Overbound Modeling of Multipath Error for Safety Critical Urban Environment, 180–194. https://doi.org/10.33012/2021.17874

Perea Diaz, S. (2019). *Design of an integrity support message for offline advanced RAIM* [Doctoral dissertation, RWTH Aachen University]. https://doi.org/10.18154/RWTH-2019-05834

Racelis, D., & Joerger, M. (2022). Evaluating New and Current Horizontal Protection Levels in the Baseline ARAIM Algorithm. *Proceedings of the 35th International Technical Meeting of the Satellite Division of The Institute of Navigation (ION GNSS+ 2022)*, 238–246. https://doi.org/10.33012/2022.18360

Rife, J., & Gebre-Egziabher, D. (2007). Symmetric Overbounding of Correlated Errors. *Navigation*, *54*(2), 109–124. https://doi.org/10.1002/j.2161-4296.2007.tb00398.x

Roberto Matera, E., Ekambi, B., & Chamard, J. (2024). A Comparative Analysis of GNSS Multipath Error Characterization Methodologies in an Urban Environment. *2024 International Conference on Localization and GNSS (ICL-GNSS)*, 1–7. https://doi.org/10.1109/ICL-GNSS60721.2024.10578540

Rößl, F., Crespillo García, O., Heirich, O., & Kliman, A. (2023). A Map Based Multipath Error Model for Safety Critical Navigation in Railway Environments. *2023 IEEE/ION Position, Location and Navigation Symposium (PLANS)*, 446–457. https://doi.org/10.1109/PLANS53410.2023.10140130

Siebert, C., Konovaltsev, A., & Meurer, M. (2023). Development and Validation of a Multipath Mitigation Technique Using Multi-Correlator Structures. *Navigation*, *70*(4), navi.609. https://doi.org/10.33012/navi.609

Teunissen, P. J., & Montenbruck, O. (2017). *Springer handbook of global navitagion satellite systems*. Springer International Publishing. https://doi.org/10.1007/978-3-319-42928-1

Working Group C (WGC) - ARAIM Technical Subgroup. (2016). Milestone 3 Report (EU-US Cooperation on Satellite Navigation, Ed.).

## A. MODIFIED H-ARAIM IMPLEMENTATION

This section presents the adaptations made to the baseline H-ARAIM algorithm using the proposed multipath error model to provide a robust error description for Section IV. A modified Horizontal Advanced Receiver Autonomous Integrity Monitoring (H-ARAIM) system is used for uncertainty quantification of the GNSS pseudorange based position solution. ARAIM is an integrity monitoring concept developed by (Working Group C (WGC) - ARAIM Technical Subgroup, 2016)) for civil aviation, with possible extension to the railway and maritime sector. The ARAIM baseline algorithm exploits redundant GNSS observations for multi-hypothesis solution separation, performing consistency checks for different fault modes $(k)$ with respect to an All-In-View solution $(k = 0)$. In addition, precise products are used in this work to correct GNSS range errors as good as possible, such that the remaining error is mostly due to the multipath and receiver noise error. In detail, satellite orbit and clock, signal biases as well as atmospheric corrections are applied. A summary of residual errors and how they are modeled is given by Table 3

**Table 3:** GNSS pseudorange error magnitude, corrections and residual error model

| Error | Magnitude [m] | Correction | Residual Error model [m] |
|---|---|---|---|
| Orbit and Clock | 2 [1] | *.sp3 and *.clk [3] | $\sigma_{\text{URA}} = 0\,1$ |
| Ionosphere | 30 [2] | Ionex file [3] | $\sigma_{\text{UIRE}} = \text{RMS}_{\text{Ionex}}$ |
| Troposphere | 6 [2] | VMF3 [4] | $\sigma_{\text{tropo}} = 0.12\frac{1.001}{\sqrt{0.002001+\sin(\theta)^2}}$ |
| User error | – | – | $\sigma_{\text{user}} = \sigma_{\text{cmpn}}$ |

[1] (Perea Diaz, 2019) [2] (Teunissen & Montenbruck, 2017)
[3] (Montenbruck et al., 2017) [4] (Landskron & Böhm, 2018)

In the following the most important steps how to incorporate the presented multipath error model are presented. H-ARAIM uses a snapshot based weighted least square (WLS) solution for the All-In-View solution with respect to an a-priori solution:

$$\delta\hat{\boldsymbol{x}} = \boldsymbol{S}^{(0)}\boldsymbol{z}, \tag{19}$$

with reduced GNSS measurements $\boldsymbol{z}$ and the projection matrix $\boldsymbol{S}$. It is defined for fault mode $(k)$ as:

$$\boldsymbol{S}^{(k)} = \left(\boldsymbol{H}^T\boldsymbol{W}^{(k)}\boldsymbol{H}\right)^{-1}\boldsymbol{H}^T\boldsymbol{W}^{(k)}, \tag{20}$$

where $\boldsymbol{H}$ is the geometry matrix with respect to local coordinates and weight matrix $\boldsymbol{W} = \boldsymbol{\Sigma}_{\text{INT}}^{-1}$. The covariance matrix of the measurements for integrity purposes $\boldsymbol{\Sigma}_{\text{INT}}$ is a diagonal matrix with elements given by:

$$\boldsymbol{\Sigma}_{\text{INT}}(i,i) = \sigma^2_{\text{URA},i} + \sigma^2_{\text{tropo},i} + \sigma^2_{\text{UIRE},i} + \sigma^2_{\text{user},i}, \tag{21}$$

with the residual error model for orbit and clock $\sigma_{\text{URA}}$, troposphere $\sigma_{\text{tropo}}$, ionosphere $\sigma_{\text{UIRE}}$ and local user error $\sigma_{\text{user}}$. The variance for the coordinate component $q \in \{1,2,3\}$ for east, north and up for the specific fault mode is given by:

$$\sigma_q^{(k)2} = \left(\boldsymbol{H}^T\boldsymbol{W}^{(k)}\boldsymbol{H}\right)^{-1}_{q,q}. \tag{22}$$

Similarly, the worst case impact of the measurement bias $b_i = b_{\text{nom},i} + b_{\text{user},i}$ is projected into the position domain via:

$$b_q^{(k)} = \sum_{i=1}^{N_{\text{sat}}} |\boldsymbol{S}^{(k)}_{q,i}| \cdot b_i. \tag{23}$$

The threshold for solution separation for each subset is given by:

$$T_{k,q} = Q^{-1}\left(\frac{P_{\text{FA},q}}{2N_{\text{fault modes}}N_{\text{ES, CONT}}}\right) \cdot \left(\boldsymbol{e}_q^T\left(\boldsymbol{S}^{(k)} - \boldsymbol{S}^{(0)}\right)\boldsymbol{\Sigma}_{\text{acc}}\left(\boldsymbol{S}^{(k)} - \boldsymbol{S}^{(0)}\right)^T\boldsymbol{e}_q\right) = K_{\text{FA},q} \cdot \sigma_{ss,q}. \tag{24}$$

The test is successful if:

$$|\hat{x}_q^{(k)} - \hat{x}_q^{(0)}| \leq T_{k,q}. \tag{25}$$

Only if all tests are successful the protection level computation can be attempted. The authors of (Racelis & Joerger, 2022) presented a new computational more efficient and tighter HPL equation, being defined as:

$$\rho_j \cdot \frac{PHMI_H}{2N_{\text{ES,INT}}} \cdot \left(1 - \frac{p_{\text{fault, not monitored}}}{PHMI}\right) = 2\overline{Q}\left(\frac{HPL - b_H^{(0)}}{\sigma_H^{(0)}}\right) + \sum_{k=1}^{N_{\text{fault modes}}} p_{\text{fault},k} \cdot \overline{Q}\left(\frac{HPL - T_H^{(k)} - b_H^{(k)}}{\sigma_H^{(k)}}\right), \tag{26}$$

where $\rho_j$ is the exclusion factor, $PHMI_H$ us the horizontal integrity budget, $p_{\text{fault not monitored}}$ is the probability of the modes to be not monitored and $\overline{Q}(u) = \begin{cases} Q(u) & u > 0 \\ 1 & u \leq 0 \end{cases}$ is the modified tail probability of a standard normal distribution and sub index $H$ denotes the horizontal coordinate component, e.g. $\sigma_{\text{H}}^{(k)} = \sqrt{\sigma_{\text{E}}^{(k)2} + \sigma_{\text{N}}^{(k)2}}$. Table 4 lists used design parameters.

| Parameter | Value |
|---|---|
| $\sigma_{\text{Ura}\|\text{Sisa}}$ | $0.1\,\mathrm{m}$ |
| $\sigma_{\text{Ure}\|\text{Sise}}$ | $0.067\,\mathrm{m}$ |
| $P_{\text{FA,Hor}}$ | $5 \times 10^{-7}/\mathrm{h}$ |
| $N_{\text{ES,INT}}$ | $450$ |
| $N_{\text{ES,CONT}}$ | $450$ |
| $b_{\text{nom}}$ | $0.5\,\mathrm{m}$ |
| $P_{\text{const,GPS}}$ | $1 \times 10^{-8}/\mathrm{appr.}$ |
| $P_{\text{const,GAL}}$ | $1 \times 10^{-4}/\mathrm{appr.}$ |
| $P_{\text{sat}}$ | $1 \times 10^{-5}/\mathrm{appr.}$ |
| FD\|FDE mode | FDE |

**Table 4:** Modified ARAIM design parameters used for presented experiments